Gravity field and rotation state of Mercury from the BepiColombo Radio Science Experiments

A. Milani[a]*, A. Rossi[b], D. Vokrouhlický[c],
D. Villani[d] and C. Bonanno[a]

[a]Dipartimento di Matematica, Università di Pisa,
Via Buonarroti 2, 56126, Pisa, Italy
[b] Istituto CNUCE-CNR, Area di Ricerca del CNR
Via Moruzzi 1, 56100, Pisa, Italy
[c]Institute of Astronomy, Charles University
V Holešovičkách 2, 18000 Prague 8, Czech Rep.
[d]Hyperborea SCRL, Polo Tecnologico
Via Giuntini 13, 56023 Navacchio, Pisa, Italy

Submitted 30 September 2000; revised 23 January 2001

*Corresponding author: Telephone: +39 050 844252 – Fax: +39 050 844224 – e-mail: milani@dm.unipi.it

Abstract

The ESA mission BepiColombo will include a Mercury Planetary Orbiter equipped with a full complement of instruments to perform Radio Science Experiments. Very precise range and range rate tracking from Earth, on-board accelerometry, altimetry, and accurate angular measurements with optical instruments will provide large data sets. From these it will be possible to study (1) the global gravity field of Mercury and its temporal variations due to tides (2) the medium to short scale (down do $300 \simeq 400$ km) gravity anomalies (3) the rotation state of the planet, in particular the obliquity and the libration with respect to the 3/2 spin orbit resonance, (4) the orbit of the center of mass of the planet.

With the global gravity field and the rotation state it is possible to tightly constrain the internal structure of the planet, in particular to determine whether the solid surface of the planet is decoupled from the inner core by some liquid layer, as postulated by dynamo theories of Mercury's magnetic field. With the gravity anomalies and altimetry it is possible to study the geophysics of the planet's crust, mantle and impact basins. With the orbit of the planet closest to the Sun it is possible to constrain relativistic theories of gravitation.

The possibility of achieving these scientific goals has been tested with a full cycle numerical simulation of the Radio Science Experiments. It includes the generation of simulated tracking and accelerometer data, and the determination, by least square fit, of a long list of variables including the initial conditions for each observed arc, calibration parameters, gravity field harmonic coefficients and corrections to the orbit of Mercury. An error budget has been deduced both from the formal covariance matrices and from the actual difference between the nominal values used in the data simulation and the solution. Thus the most complete error budget contains the effect of systematic measurement errors and is by far more reliable than a formal one. For the rotation experiment an error budget has been computed on the basis of dedicated studies on each separate error source.

The results of the full cycle simulation are positive, that is the experiments are feasible at the required level of accuracy. However, the extraction of the full accuracy results from the data will be by no means trivial, and there are a number of open problems, both in the data processing (e.g., the selection of the orbital arc length) and in the mission scheduling (e.g., the selection of the target areas for the rotation experiment).

1 Introduction

The European BepiColombo mission will be launched in the year 2009, and will achieve orbit insertion around Mercury at some time in 2011 (or perhaps in 2012, depending upon the selected launch window). The innermost planet of the solar system was last visited by Mariner 10 in 1974-1975. With its small fleet of three spacecraft and a large complement of advanced scientific instruments, BepiColombo should provide a huge leap forward in our knowledge of Mercury and, as a consequence, in our understanding of the structure, formation and evolution of the terrestrial planets.

This paper is specifically dedicated: first, to the definition of the goals to be set for the understanding of the internal structure of the planet, from the point of view of gravimetry, geodesy and solid geophysics; second, to describe the experimental method, the so called Radio Science Experiments, to be used to obtain the necessary measurements; third, to the assessment of the possibility to achieve the stated goals with the available resources. This assessment has been conducted by means of a full cycle numerical simulation of the experiments. Besides the simulation results we discuss the difficulties found in the processing of the simulated data (which presumably would occur also in the processing of the real data), the main limiting factors controlling the accuracy of the results, and some possible ways to remove these limitations to further increase the science return.

We anticipate that the results of the simulations have been favorable, that is the scientific goals are achievable with the proposed instrumentation. However, the task of actually extracting the full accuracy results from the data appears far from trivial, and we cannot claim that we have solved all the problems, which will require an additional research effort, to be conducted in the years between now and 2011.

1.1 Science background

The gravity field of Mercury is essentially unknown. The tracking data from the three fly-by of Mariner 10 in 1974-75 have been reanalyzed (Anderson *et al.*, 1987), to give a low accuracy estimate of the normalized degree 2 coefficients $C_{20} = -(2.7 \pm 0.9) \times 10^{-5}$ and $C_{22} = (1.6 \pm 0.8) \times 10^{-5}$ (values in the body-fixed frame of the principal axes of inertia tensor). This level of knowledge does not allow to constrain in a significant way the internal structure of the planet. Moreover, already Newton (1687) had shown that no amount of information on the gravity field – measured outside the body of the planet – can be sufficient to reconstruct the internal mass distribution in an unique way. In fact there is no way to determine uniquely the internal structure by remote sensing; but, it is possible to strongly constrain the models of the interior if the low degree coefficients of the gravity field are accurately determined, and at the same time the rotation state of the planet is accurately determined (Spohn *et al.*, 2001). In simple words, knowing in which way the rotation state of the planets reacts to external torques (in this case, to the differential attraction from the Sun), and also knowing the low degree gravity field, allows to solve for the principal moments of inertia of the planet. If the planet has a liquid layer, completely decoupling a more or less rigid crust from a solid core, it is possible to separately estimate the moment of inertia of the solid layer above the liquid interface. Moreover, accurate measurements of the low degree and order (2–4) coefficients of the development in spherical harmonics of the gravity field impose global evolutive constraints. The static part of the field provides information on how the global shape of Mercury has been affected by the solar tide over its history, while the time-dependent part, parametrized mostly by the Love number k_2, provides information on the elasticity of the response of the bulk of Mercury to externally induced deformations.

Lateral inhomogeneities in the mantle at a wavelength comparable to the height of the orbiter above the surface could be deduced from high order harmonics (from this point of view, the measurements performed near the pericenter are the most useful). By analogy with the Moon, we may ask whether Mercury has "mascons", large positive anomalies in density at comparatively low depths (50 – 100 km). The lunar mascons are well understood in terms of infiltration of basaltic lava with a density higher than that of the crustal rocks. This results from the fracturing of the crust, down to the crust-mantle interface, by a large impact. Since the thickness of the crust of Mercury is very poorly constrained at present, and since the albedo/color contrast between the supposed maria of lava and the highlands is much less on Mercury, we have no way to predict quantitatively what a gravity map of the planet could reveal. However, the absence of mascons would be very surprising. Thus we can only propose to measure, as well as the orbital configuration allows us, the local gravity anomalies. The depth of the crust-mantle interface can be constrained using the gravity and the topography data from the altimetry, with the assumption that the local variations of the gravity field are caused by variations on the crust thickness.

1.2 Statement of objectives

The goals of the Radio Science Experiment can be qualitatively described as follows:

1. to measure the rotation state of Mercury, to an accuracy allowing to constrain the size and physical state of the core of the planet;

2. to measure the global structure of the gravity field of Mercury, to an accuracy allowing to constrain the internal structure;

3. to measure the local gravitational anomalies of Mercury, to an accuracy allowing to constrain the structure of the mantle, the crust/mantle interface, and characterize the mascons;

4. to measure the orbit of Mercury around the Sun and the propagation of radio waves between the Earth and Mercury in order to test general relativity to an unprecedented level of accuracy through improving constraints on the post-Newtonian parameters.

Note that the last of these goals is outside the scope of this paper; it is discussed in Iess *et al.* (2001) and Milani *et al.* (2001).

To give quantitative statements of the first 3 goals we need to introduce the normalized harmonic coefficients $C_{\ell m}, S_{\ell m}$ of Mercury's gravity potential

$$U = \frac{GM}{R} \sum_{\ell m} \left(\frac{R}{r}\right)^{\ell+1} P_{\ell m}(\sin\theta) \ \left[C_{\ell m}\cos(m\lambda) + S_{\ell m}\sin(m\lambda)\right] \ ,$$

where G is the gravitational constant, M, R are the mass and the radius of the planet, r the distance from the center, λ, θ the longitude and latitude, $P_{\ell m}$ the normalized Legendre function, ℓ is the degree and $m \leq \ell$ the order. The resolution of the gravity filed modeled by harmonics up to degree ℓ is $\pi R/\ell$. The goal of a gravimetry experiment can be expressed in terms of the signal-to-noise ratio; by this we mean the ratio between the expected coefficients at a given degree ℓ and the error, including random error and systematic error, in the same coefficients. For BepiColombo, with a pericenter of the orbit at 400 km altitude, the goal should be to have a signal one order of magnitude above the noise at the degree corresponding to a resolution of 400 km, that is $\ell \simeq 20$. The signal, that is the harmonics of the gravity field of Mercury, is of course unknown, but the order of magnitude is predicted by the so called

Kaula's rule (Kaula, 1966) by which the average (in the RMS sense) value of the coefficients of degree ℓ is $\simeq c/\ell^2$. The value of the constant c has a value depending upon the planet: $c \simeq 8 \times 10^{-6}$ for Earth, $c \simeq 10^{-5}$ and Venus, $c \simeq 10^{-4}$ for Mars, $c \simeq 3 \times 10^{-4}$ for the Moon. Since c scales roughly with the inverse of the surface gravity (Vincent and Bender, 1990) we can expect for Mercury $c \simeq 3 \times 10^{-5}$.

For the low degree harmonics, a much better relative accuracy is required to constrain the models of the planetary interior; the signal-to-noise required is about 10^3 for degrees 2 to 4. The Love number k_2 and the corresponding dissipation factor Q_2 are measures of the response of the solid body of Mercury to the tidal deformation induced by the Sun; for precise definitions see Munk and Macdonald (1960, Chap. 5). They appear in the equations of motion of a satellite of Mercury as time variations of the harmonic coefficients of degree $\ell = 2$ depending upon the mercurycentric position of the Sun. The Love number k_2 for the Earth is $\simeq 0.3$, while the dissipation factor $Q_2 \simeq 20$ (at very low, tidal frequencies); is it not easy to predict the values for Mercury, but the dissipation factor should be significantly larger, hence the phase lag of the solid tidal wave is very difficult to measure. The value of k_2 is an important constraint in the models for the interior of Mercury (Spohn *et al.*, 2001), thus it would be desirable to measure it with an accuracy of 1% or better.

To describe the rotation of the planet we need to refer to the principal moments of inertia A, B, C of the planet; C is the largest one, corresponding to an axis close to the rotation one. If a solid upper layer is decoupled from a solid inner core by a complete liquid layer, the largest moment of inertia C_m of the solid upper layer alone can be measured independently (Peale, 1976). This will be described in Section 5. A significant goal would be to measure the ratio C_m/C, which would be 1 for a frozen solid planet, and is expected to be $\simeq 0.5$ for a planet with an important liquid layer, with an accuracy of 0.05 (i.e. $\approx 10\%$ of the quoted range).

The degree of mass concentration towards the center of the planet is measured by the *concentration coefficient* C/MR^2, whose value is an important constraint to the size and density of the core; the value is 0.4 for an homogeneous planet, and is expected to be significantly less for Mercury; a significant goal would be to measure this to an accuracy of 0.003, which means $\simeq 1\%$ of the expected value.

1.3 The Radio Science Experiments

The Radio Science Experiments are a complex of measurements and scientific goals; note that it is not possible to separate them neatly in independent experiments, but each one of them depends to some extent upon the intermediate and final results of the others. Nevertheless we can distinguish a *gravimetry experiment*, with the goal of determining the gravity field of Mercury; a *rotation experiment*, with the goal of determining the rotation state of Mercury, and a *relativity experiment*, with the goal of determining the post-Newtonian parameters and other quantities of interest in the very accurate dynamic modeling of the solar system, such as the mass and the dynamic oblateness of the Sun.

The basic idea is as follows. The BepiColombo Mercury Planetary Orbiter (MPO), the main spacecraft of the mission, will be tracked from ground antenna(s) with a ultra stable multiple frequency radio link; range and range-rate will be thus measured with great accuracy (the expected RMS are a few tens of cm and a few tens of micron/s). Note that these are among the most accurate measurements in all fields, at the level of 1 part in 10^{12} for range and a few parts in 10^{10} for range-rate.

This will allow an extremely accurate orbit determination, which in fact will result in three separate data products (Section 3):

1. the initial conditions of the mercurycentric orbit of the spacecraft, for each short arc corresponding to an observing session from the ground antenna (see Section 2.1);
2. the corrections to the orbit of Mercury;
3. the parameters appearing in the equations of motion of the spacecraft, including the harmonic coefficients of the planet's gravity field and the nongravitational perturbations.

The nongravitational perturbations, particularly strong in the intense radiation environment of Mercury, can be removed from the list of unknowns by replacing them with the reading of the on-board accelerometer (in fact, some of the unknown parameters are replaced by the calibration coefficients of the instrument, see Section 2.2, but the number of unknowns is sharply reduced). In this way not only the orbit of the spacecraft (and that of Mercury) is better determined, but especially the effects of the gravitational anomalies are well isolated by any other perturbation which can act with similar effects.

Since the pericenter of the MPO will be at an altitude of 400 km, its orbit will be mainly sensitive to gravity anomalies with a scale equal or larger than about 400 km. However, the MPO will have a moderately elliptic orbit, with apocenter at an altitude of 1500 km. The orbit will be polar, with pericenter always located at a low latitude (between 17° South and 17° North), thus the surface of the planet will be over flown at such a low altitude only over a latitude band around the equator. However, we have checked that the entire surface will be over flown at less than 750 km altitude: the polar regions will be covered more often but from somewhat higher altitude, which results in some compensation. The tracking data, especially the range-rate, taken during the low portion of the orbit will be most sensitive to the gravity anomalies of degree up to $\ell = 20$. The tracking data taken during the high portion of the orbit will be more sensitive to the low degree harmonics, and to the Love number k_2. With all that, the data processing needs to be done in a single global least squares fit, and all the harmonic coefficient, calibration coefficients, initial conditions, and Mercury orbit corrections will be solved at once.

The Mercury orbit corrections will then be fed as input to a fit solving for the orbit of the planets Earth and Mercury, and for the relativistic post-Newtonian parameters (Iess *et al.*, 2001; Milani *et al.*, 2001). Since the poorly known quadrupole coefficient of the solar gravitational field can produce a measurable effect at the level of precision of the BepiColombo tracking, we consider it as a solved-for parameter as well. Similarly, a small adjustment of the solar mass (or equivalently the astronomical unit which is presently known with a precision of ≈ 30 m) is also allowed.

The initial conditions of the mercurycentric orbit of the MPO, available for every short observed arc, can be propagated to estimate the position of the spacecraft even outside of the observation sessions. The accuracy is of course degraded, e.g., tens of meters rather than the tens of centimeters possible within the observed arcs; but still the MPO will be an extremely stable platform realizing very accurately an absolute, inertial reference system. From this platform a high resolution camera (which of course is also used for mapping the planet) will repeatedly look at a number of patches on the surface.

The pointing direction of the camera will be well known, because a star mapper (and/or possibly another camera, expected to search for Near Earth

Objects) will define the orientation of the spacecraft in a stellar reference frame, which in turn is related to an inertial frame by star catalogs containing good proper motion data (e.g, the ones exploiting the results from Hipparcos). This allows to compute the direction from the MPO to a specific footprint on the surface; by correlating two images it is possible to directly measure the rotation of the planet in the inertial frame defined by the MPO and the stars.

Once the rotation state of the planet is known, the values of the obliquity η and of the libration in longitude β will be used together with the values of the degree $\ell = 2$ harmonic coefficients to solve for both C/MR^2 and C_m/C; the relevant equations are given in Section 5.

Organization of the paper

Section 2 discusses the two main data set we expect to have available from the BepiColombo Radio Science measurements, their temporal structure and the noise models. In Section 3 we discuss the determination of the mercurycentric orbit of the spacecraft. Section 4 presents the results on the gravity field of Mercury, while Section 5 discusses the rotation experiment. The conclusions are outlined in Section 6, together with indications for the work to be done to be ready for the arrival of BepiColombo at Mercury.

2 The measurements

To measure the gravity field and the rotation state of Mercury we have to perform an accurate orbit determination of both the spacecraft and the planet, and to measure the orientation of the solid surface of Mercury in an inertial reference frame. To accomplish this task we make use of the following observable quantities:

1. the range and range-rate between the ground station(s) and the spacecraft, provided by the ground station by using the on-board multi-frequency transponder (Iess *et al.*, 2001);

2. the nongravitational perturbations acting on the spacecraft, given by the on-board accelerometer (Iafolla and Nozzoli, 2001);

3. repeated images of selected areas on the surface of Mercury, taken from the spacecraft with the high resolution camera (Balogh *et al.*, 2000, Section 3.1.2);

4. images of the sky with reference stars, taken from the spacecraft with either the star mappers (Balogh *et al.*, 2000, Section 6.4.5) or the NEO telescope which has been proposed as an additional instrument.

Note that in this context by spacecraft we mean only the Mercury Planetary Orbiter (MPO), since the Mercury Magnetospheric Orbiter (MMO) is not equipped with the necessary instrumentation (Ka-band transponders and accelerometer, high resolution camera and star mapper) to achieve top accuracy in the Radio Science Experiments.

The first step in a simulation of the Radio Science Experiments is to simulate the data set which will be available from all types of measurements. The datasets 3 and 4 are used only in the rotation experiment, and they will be discussed in Section 5; the datasets 1 and 2 are used in all the Radio Science Experiments, and are described in this section.

2.1 Range and range-rate

The range and range-rate between the ground station(s) and the spacecraft are obtained by means of a multi-frequency link in X and Ka-bands, allowing to remove the effects of the ionospheric and coronal plasma along the path, provided by a high stability transponder on board (Iess *et al.*, 2001).

Visibility conditions

While the transponder could, in principle, provide continuous measurements, the relative position and motion of the ground antenna(s), the spacecraft, Mercury and the Sun limit the actual measurement time to selected intervals. Studying the time evolution of the complex geometry of the system (Fig. 1) the visibility conditions of the spacecraft from the ground antenna can be determined.

In the simulations we made the (worst case) assumption of having just one ground station available, located in Perth, Australia. From this station we assumed to have range-rate measurements taken whenever possible, while the range measurements were taken during only 2 minutes every 15 minutes, to minimize the impact on the downlink data rate (see Balogh *et al.*, 2000,

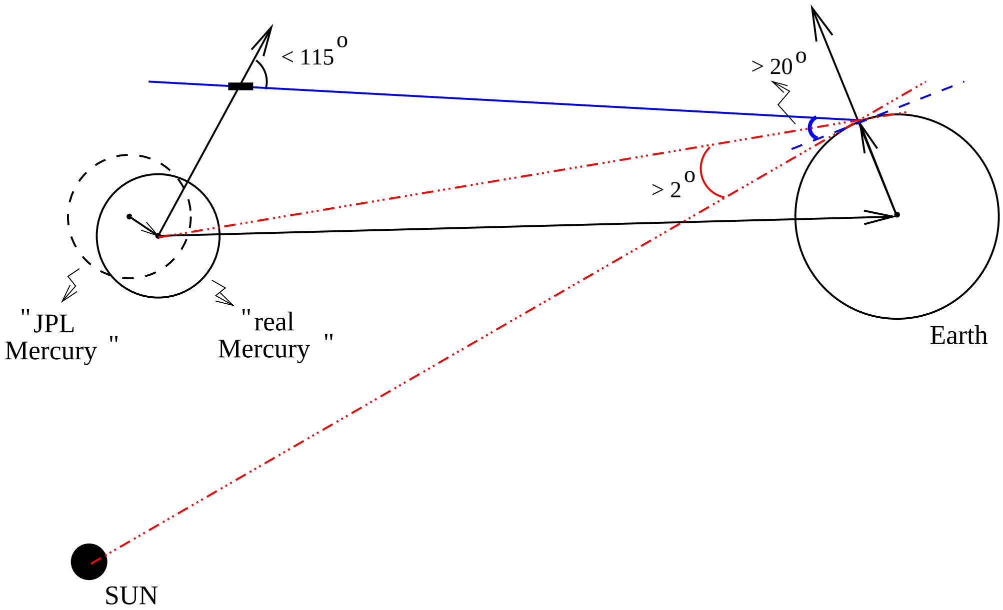

Figure 1: Geometry of the system, given by the ground station, Mercury and the Bepi-Colombo spacecraft, determining the visibility conditions.

Section 6.4.4). As mentioned above, given the relative position of the planets, the Sun and the probe, the link between the station and the satellite may not be always possible. In particular, in order to establish the visibility conditions from the ground station we took into account the following limitations:

- antenna pointing limitations: the observations are not possible when the angle between the on-board antenna axis (which is always pointed in the direction opposite to the center of Mercury) and the ground station becomes larger than a threshold value (115° for the current design, see Balogh *et al.*, 2000, Fig. 6.4-19). This condition includes the case of the satellite eclipse behind Mercury;

- ground antenna elevation limit: the antenna cannot be operated if the elevation of the satellite above the horizon is lower than a given value; we have set this value to 20° to discriminate against data which could be of lower accuracy due to errors in the models for tropospheric propagation;

- Sun corona limitation: the ground antenna cannot be aimed directly to the Sun, the offset angle has a minimum value. The use of dual band tracking allows to maintain the accuracy of the range and range-rate even when the radio waves are passing at a few radii of the Sun above the corona. In the simulation we have used the conservative assumption that this offset must be above 2°.

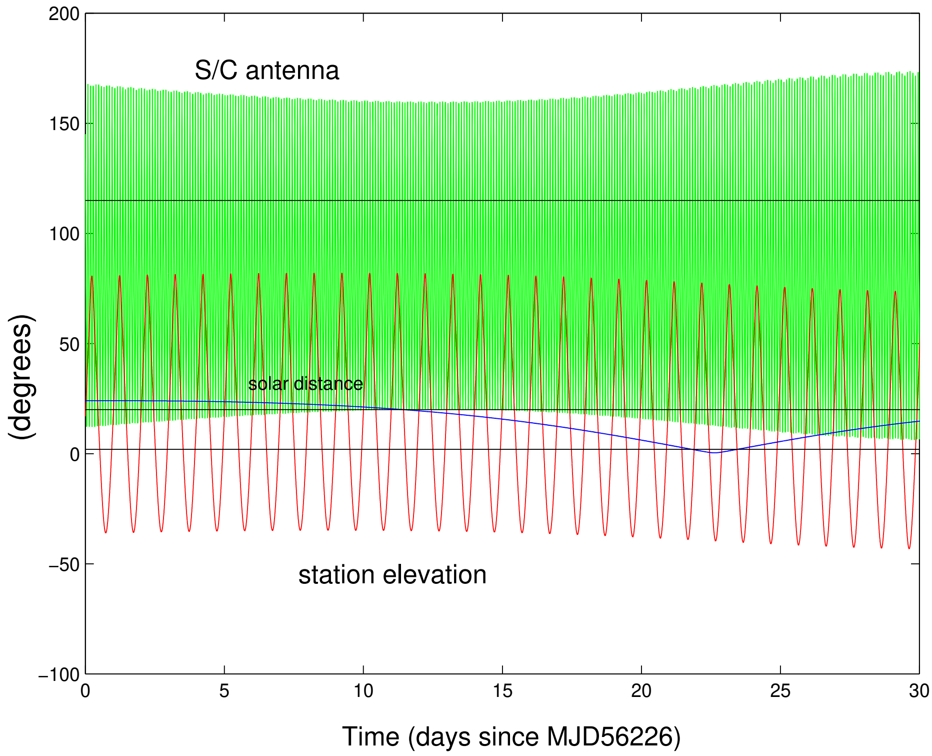

Figure 2: Visibility conditions for an interval of 30 days. Middle line (slowly varying): angular distance between the ground antenna line of sight and the direction to the Sun. Bottom line: elevation angle at the ground antenna. Top line (high frequency): angle between the ground antenna line of sight and the spacecraft antenna axis (see Fig. 1). The threshold values for these three angles are marked with solid lines at 2°, 20° and 115° respectively.

The time evolution of these limiting conditions were studied during a one year data simulation; the spacecraft antenna visibility conditions are summarized in Figs. 2 and 3, for a time span of 30 and 365 days respectively. In the plots, the horizontal solid lines set the limits for the three conditions described above. The curved line in the middle denotes the angular distance between the ground antenna line of sight and the direction to the Sun. The

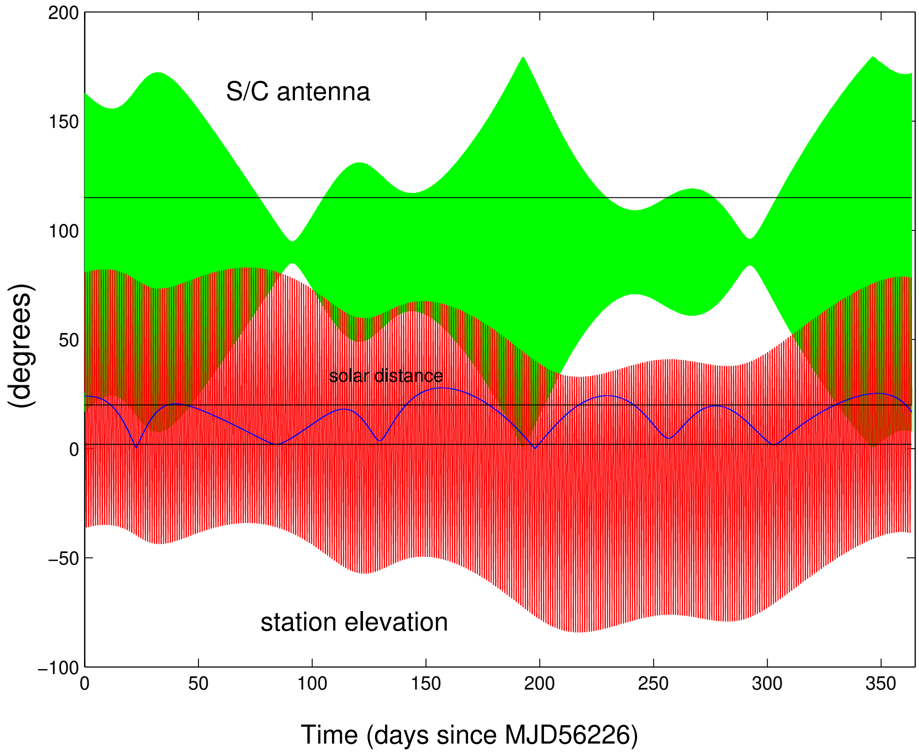

Figure 3: Visibility conditions for an interval of 365 days, with the same conventions as in the previous Figure. Visibility of Mercury from the ground station is better in the first 100 days of the mission, which correspond to late spring and summer at the Australian ground station. Occultations by the planet Mercury do not occur when the direction to the Earth is almost orthogonal to the spacecraft orbit plane, between days 200 and 310. The Sun corona limitation is relevant only during six short intervals of time near conjunctions.

constraint on this angle is not very demanding: the line lies almost always above the $2°$ limiting value. The bottom line gives the elevation angle of the ground antenna and the top line denotes the angle between the ground antenna line of sight and the spacecraft antenna. These two constraints are satisfied only for a limited amount of time (the most stringent being the elevation of the ground antenna). Since a measurement is possible only when all the three visibility conditions are satisfied, it turns out that the probe is tracked by the ground station only for the 26% of the time during a one year simulation time span.

Plots such as the Figs. 2 and 3 clearly show the interplay of three periods: the orbital period of the spacecraft around Mercury (2.3 hours for the Mercury Planetary Orbiter), the rotation period of the Earth (resulting in 8–10 hours observing sessions for the ground antenna) and the synodic period of Mercury with respect to the Earth. Moreover, the orbital plane of the mercurycentric orbit hardly precesses, thus there are effects with period one year, related to the angle between the Mercury-Earth direction and the orbital plane: e.g, occultations by the planet Mercury do not occur when the direction to the Earth is almost orthogonal to the spacecraft orbit plane.

Note that the transit time of the light from the ground to the probe is not negligible (on average 8 minutes) and was taken into account in the computation of the visibility conditions, and in all the simulations. This requires a substantial change in the standard algorithms used in satellite geodesy. For a satellite of the Earth the light travel time is very short with respect to the orbital period, and even with respect to the integration step size, while in this case the state of the spacecraft needs to be interpolated at a "radio waves arrival time". The algorithms to be used are very similar to the ones used for the processing of interplanetary radar data (Yeomans *et al.*, 1992).

The arc length problem

The measurement process has been divided in time intervals, each called an *arc*. This is not just an arbitrary partition of the dataset; for each arc we compute a separate set of initial conditions, as if the spacecraft orbit was not causally connected. The purpose of this over-parameterization is to absorb the unmodeled perturbations, which accumulate with time and would make impossible to solve for a purely deterministic orbit over much longer arcs. The motivation and the algorithm of this *multiarc method* are discussed in Milani *et al.* (1995). This procedure works even if the mission duration is cut into arcs of arbitrarily selected length (as in Albertella *et al.*, 1998); however, it works better if the arcs correspond to time intervals in which there are many observations, separated by "dark" intervals with no observations. Thus the partition into arcs needs to take into account the time structure of the visibility of the spacecraft. There are two obvious solutions in the case of an orbiter around Mercury:

- the arcs could be terminated whenever one of the three visibility conditions fails; these we call *very short arcs*;
- the arcs could be terminated only by the setting of Mercury below

the horizon, as seen from the station (or anyway below the minimum acceptable elevation, we have assumed 20°); these we call *short arcs*.

Assuming a single ground station, the typical length of a short arc is around 8 hours; note that, due to the occultations of the probe behind Mercury, the range-rate observations within such an arc are not continuous, but the eclipse periods are less than 1 hour.

The typical length of a very short arc is between 1.5 and 2 hours, less than an orbital period. There are even "extremely short" arcs, resulting from an eclipse occurring near the station horizon crossing, lasting 0.5 hours or even less. On the contrary, when the mercurycentric orbital plane is roughly orthogonal to the Earth-Mercury line of sight (see the interval between days 200 and 310 in Fig. 3) there are no eclipses and a very short arc is actually the same as a short arc.

As it will be clear from Sections 3 and 4, the choice between short and very short arcs is critical to achieve the best results in determining the parameters of interest, for both the gravimetry and the relativity experiments. For the rotation experiment somewhat longer arcs will be considered in Section 3.2.

The attitude/orbit maneuvers performed with jets are cause for concern; while orbit maneuvers are infrequent, the attitude ones are required to discharge the reaction wheels; they also result in changes of linear momentum because the jets are never exactly aligned and do not give the same impulse. Their number and collocation in time with respect to the ground station operating schedule need to be controlled carefully, because they could also result in a decrease of the effective duration of the orbital arcs. The rotation experiment, which needs to propagate the knowledge of the spacecraft position over time spans beyond the observing sessions, could also be affected.

Error model

A non-trivial noise model (i.e., not just white noise) was applied in the simulation of the range and range-rate observations; it is justified, both by the physical models and by experience, and discussed in detail by Iess *et al.* (2001). Fig. 4 shows the behavior of the noise during the one year simulated time span. The RMS values are 10 cm for range and 18 micron/s for range-rate, but the noise model is correlated and the RMS is not enough to define it. For the range-rate, the noise is obtained (by inverse Fourier transform) from a noise spectrum containing separate components accounting for the known physical sources of error, e.g., interplanetary plasma, the Earth's troposphere, transponder noise, etc.. For the range, a random noise is superimposed upon a constant offset plus a quadratic drift. The long term drift, clearly visible in Fig. 4, results from the assumption of component degradation in the transponder. This systematic drift in the range measurements has a very critical role in the relativity experiment, but it turns out to have little impact on the gravity and rotation experiments, which essentially use the range-rate data.

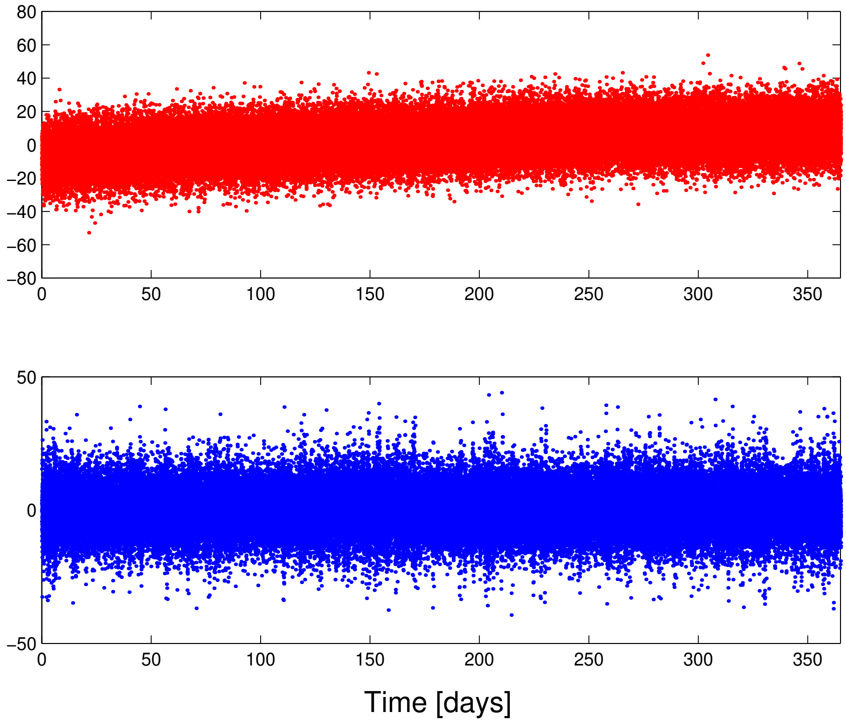

Figure 4: Noise model for the on-board transponder; the top panel shows the noise in the range measurements, in centimeters, and the bottom one shows the noise in the range-rate measurements, in micrometers per second.

2.2 Nongravitational accelerations

The accelerometer measurements were assumed to be continuous, with an integration time of 20 seconds. There is no interruption of the measurement when the spacecraft is not visible from the ground station because the data can be easily stored.

Accelerometer calibration and noise

Again, a non-trivial model was used for the instrument noise. Fig. 5 shows the behavior of the accelerometer noise during the simulated time span of one short arc. The physical model justifying this error model, and the results of the long term ground tests of the Italian Spring Accelerometer (ISA) are described in Iafolla and Nozzoli (2001).

The calibration of the accelerometers is always a thorny issue, because all accelerometers perform only relative measurements. The calibration formula for ISA is as follows

$$y = ax + bT + c + \dots \ ,$$

where x is the accelerometer reading, y is the absolute acceleration to be measured, a is a scale coefficient which is calibrated in flight to an accuracy sufficient for the purpose of this experiment, and T is the temperature. The dots stand for nonlinear effects and short period noise which are known (from the ground tests) to be smaller than the required accuracy. The coefficient $b = 5 \times 10^{-4}$ cm s^{-2} degree^{-1} is well known from ground measurements, but the absolute value of the temperature is not easy to measure with the necessary accuracy and the absolute calibration c is unknown (its value in space is anyway different from the one which could be measured on the ground). Thus the procedure needs to involve a *digital calibration*, that is the composite $d = bT + c$ is added to the variables to be determined in the least square fit.

The critical issue is how d can change with time. Experience with this (and other) accelerometers indicate that the calibration in this sense does not change on time scales shorter than 10^4 seconds, apart from the changes resulting from temperature variations. The latter occur mostly over time scales comparable to the orbital period and longer. The changes in the heat flow on the external surface of the spacecraft occur mainly with the orbital period, because of the changes in the spacecraft attitude with respect to the Sun and in the illuminated portion of the Mercury surface which is visible. Since the spacecraft is very strongly insulated, it has a huge thermal inertia and the short term changes in the heat flow result in very small changes in the internal temperature. Thus it is possible to assume d as a constant over one very short arc; the case of the short arcs is more critical, as will be shown

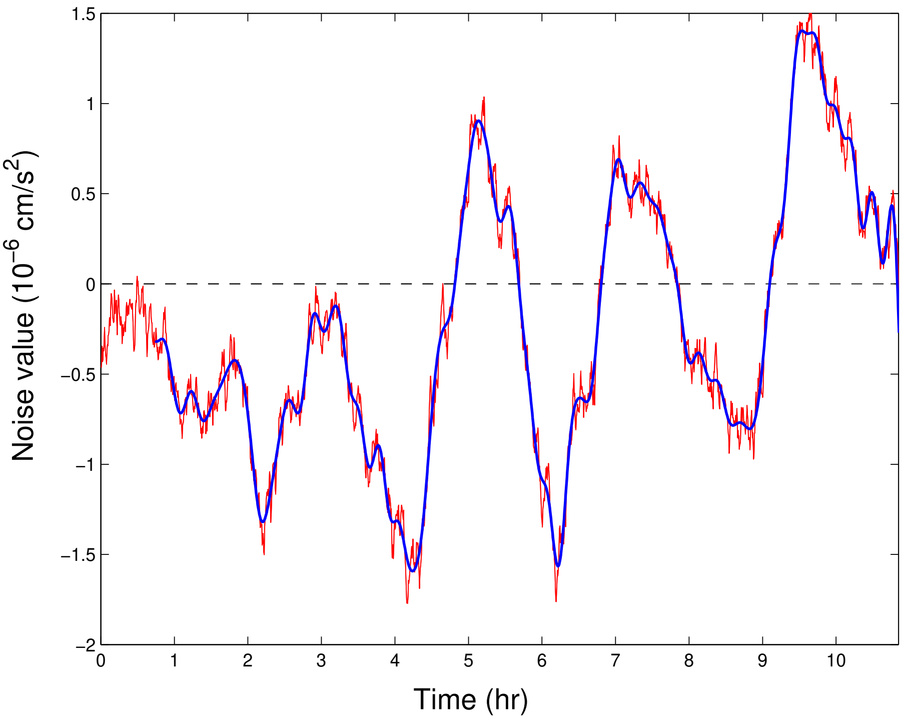

Figure 5: Accelerometer noise model, in units of 10^{-6} cm/s^2. The grey line shows the original noise, as given by the adopted model, while the black thick line shows the filtered noise, with the short period components smoothed.

later. We have already experimented, in the BepiColombo simulations, with this digital calibration and found that the addition of the corresponding d variables to be solved has indeed improved the results.

Thus we have assumed an error model of the accelerometer measurement consisting of noise correlated over time scales of the order of the orbital period, as in Fig. 5, simulating thermally driven changes to the calibration. However, the digital calibration removes the effects with longer time scales. The short period variations, simulating instrumental noise, are visible in the grey curve, and were smoothed by means of a low-pass filtering of the signal; we used a finite impulse response (FIR) linear filter (Carpino *et al.*, 1987). This smoothing was necessary to avoid instability in the numerical integrator used to propagate the orbit of the spacecraft, and does not decrease the accuracy of the orbit because the high frequency components are mostly noise, and anyway would result in very small displacements.

It turns out, as discussed in Section 4, that the systematic components of the acceleration noise are the most important cause of the systematic errors in the results for the determination of the gravity field. A simulation based upon the assumption of Gaussian uncorrelated noise would have given results with illusory precision. This also implies that an improvement in the performance of the accelerometer, and a better understanding of its error model allowing a better absolute calibration, would allow to obtain in the gravimetry experiment results even better than those presented in Section 4.

3 Orbit determination

After the data simulation process described in Section 2 the available data consist of range-rate measurements (a data every 20 seconds, taken whenever possible) and range measurements (a data every 20 seconds, but taken during only 2 minutes every 15 minutes), plus the filtered accelerometer data (continuous with a point every 20 seconds). The acceleration data are fed into the corrector to compensate for the inaccuracy of the dynamical modeling of the nongravitational perturbations.

In the algorithm to obtain a least square fit of the range and range-rate measurements there is a first necessary step. We need to solve for the initial conditions of the spacecraft mercurycentric orbit. This is indeed possible, with a standard least squares fit algorithm; for each orbital arc, the linearization of the problem consists of linear equations with coefficients forming a 6×6 matrix, the *normal matrix* N, which has to be inverted to obtain the *covariance matrix* Γ. The problem is that the normal matrix turns out to be very poorly conditioned (with very large ratio between the largest and the smallest eigenvalue); as a result, there is a loss of precision, that is the uncertainties in the initial conditions are much larger than the uncertainties in the measurements.

This phenomenon has to be fully understood; first, because without a modification of the algorithm allowing to stabilize the orbit determination, the results of all the Radio Science Experiments would be degraded; second, because this problem is intrinsically related to the geometry of the observation and orbit determination process, as opposed to a numerical accuracy and/or software problem. The next subsection introduces the mathematical theory of this effect and indicates some of the possible solutions.

3.1 Rank deficiency

In the process of orbit determination of an object moving in outer space, be it a spacecraft or a natural body (e.g., a planet), the problem of *rank deficiency* often occurs. In the extreme case, the normal matrix N (of type $n \times n$) has a rank $r < n$ and it cannot be inverted at all; this implies that the least squares fit has a solution on a set not consisting of a single point, but containing a manifold with dimension $n - r$. In a more common case, N is non degenerate, but has $n - r$ eigenvalues which are smaller than the largest one by many orders of magnitude.

This phenomenon can be explained by finding a symmetry group G, such that the action of the group on the space of the parameters to be solved does not change at all the *target function* Q (the sum of the squares of the residuals). In this case all the values of the parameters which can be obtained by the group action starting from some minimum of Q are also minima, and the dimension of this set of solutions is the rank deficiency $n - r$. Let us assume that the symmetry is broken, but still holds approximately, that is, by applying to the minimum the symmetries the target function Q increases by a very small amount, of the order of ϵ^2, where ϵ is a small parameter. Then the normal matrix will have an eigenvalue of the order of ϵ^2, and the poor conditioning of N will result in a loss of precision, amplifying the uncertainty by a factor of the order of $1/\epsilon$.

The case of an orbiter around another planet, e.g. Mercury, tracked from the Earth by means of range and range-rate measurements, has been rigorously studied (Bonanno and Milani, 2001). This problem has an exact rank deficiency in the simplified case where (i) the planet has a spherically symmetric gravity field (ii) the length of the arc for which initial conditions are determined is negligible with respect to the orbital motions of the Earth and of the planet. In this ideal case the rank of the normal matrix is 5, that is, only five orbital elements can be determined. If mercurycentric Keplerian orbital elements are used, with the reference plane orthogonal to the Earth-Mercury line of sight, then the longitude of the node Ω cannot be solved by least squares fit.

If the change in the Earth-Mercury direction, within the time span of the arc, is by an angle ϵ, then the normal matrix has an eigenvalue of the order of ϵ^2; an explicit estimate is available. Also the oblateness of the planet results in symmetry breaking, but, in the case of a Mercury orbiter, its contribution to the increase in the target function is less important.

Two conclusions can be drawn from this theoretical analysis. The approximate rank deficiency could be completely eliminated by using orbital arcs, for which a single set of initial conditions is determined, with a length comparable to the synodic period of Mercury (with respect to the Earth). This is not possible: over an arc of several weeks the systematic errors in the orbit determination resulting from dynamic model errors (mainly nongravitational perturbations) would by far exceed the loss of precision occurring in short arcs. Then it is necessary not to attempt a fully independent orbit determination for a short arc; the sixth orbital element needs to be constrained by means of information obtained from longer arcs, even if this constraint has in itself lower accuracy. Among the different algorithms available to perform this constraint (discussed in Bonanno and Milani, 2001) we have used the simplest one, the standard collocation method: some a priori knowledge of all the initial conditions is assumed, at levels of accuracy compatible with the systematic errors in the dynamic model for arcs spanning several days.

In a complete treatment of the orbit determination around another planet we should include the uncertainty on the orbit of the planet around the Sun. In the case in which this uncertainty is bigger than the accuracy of our observations, this would require to determine, for each arc, also six orbital elements of the planet. Another approximate symmetry, again intrinsic in the geometry of the problem, would then result in a loss of precision. This new symmetry, together with the previously studied one, would lead to a 12×12 normal matrix N with 5 eigenvalues much smaller then the largest one, that is we would have an approximate rank deficiency of 5. This would negatively affect the precision of both the mercurycentric orbit of the spacecraft and the heliocentric orbit of Mercury.

This problem is solved by correcting the heliocentric position and velocity of the planet only in the direction of the Earth-planet line of sight. Thus each arc has only 8 local parameters, out of which 2 are indirect measurements of the range and range-rate to the center of mass of the planet, to be used in the orbit determination of Mercury for the purpose of the relativity experiment, as described in Milani *et al.* (2001).

3.2 Results and problems

In the simulation of the differential correction process we have assumed an a priori knowledge of the initial mercurycentric position with an RMS of 3 meters in each coordinate, and 3 meters per day in each coordinate of the

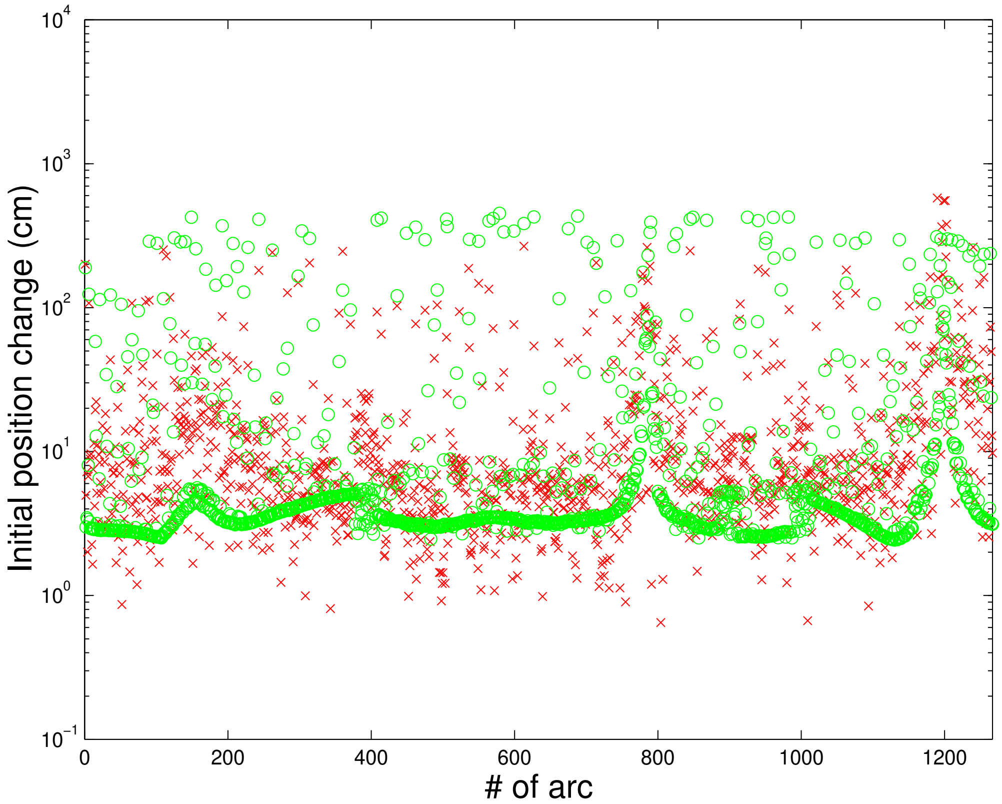

Figure 6: Formal uncertainties (circles) and actual errors (crosses) in the initial conditions determination for each arc, in the very short arc case. The arcs cover one year (nominal mission duration).

velocity.

As pointed out in Section 2.1, we can work with two kind of arcs: *short* and *very short*. In the first case the simulation produced 353 arcs, while in the second one we are dealing with 1267 arcs, covering a one year nominal mission duration.

In Fig. 6 we summarize the results of the initial conditions determination for very short arcs. For each arc, the circles represent the formal uncertainty of the initial condition determination, while the crosses give the "real" error, obtained as difference between the initial conditions used in the data simulation and the values determined in the fit; the latter take into account all the systematic error components. The spacecraft orbit can be usually determined very well; nonetheless we note that there are many arcs for which both the formal uncertainty and the error are large. These are generally "extremely short" arcs, during which the angular displacement of Mercury is very small, hence the rank deficiency is close to an exact one. In fact there are many arcs for which the formal position uncertainty is about 3 meters. This can be understood by thinking to the case in which the eigenspace of the normal matrix corresponding to an eigenvalue of the order of ϵ^2 is along one of the coordinate axis: then the knowledge of that coordinate would not be improved at all with respect to the 3 meters a priori.

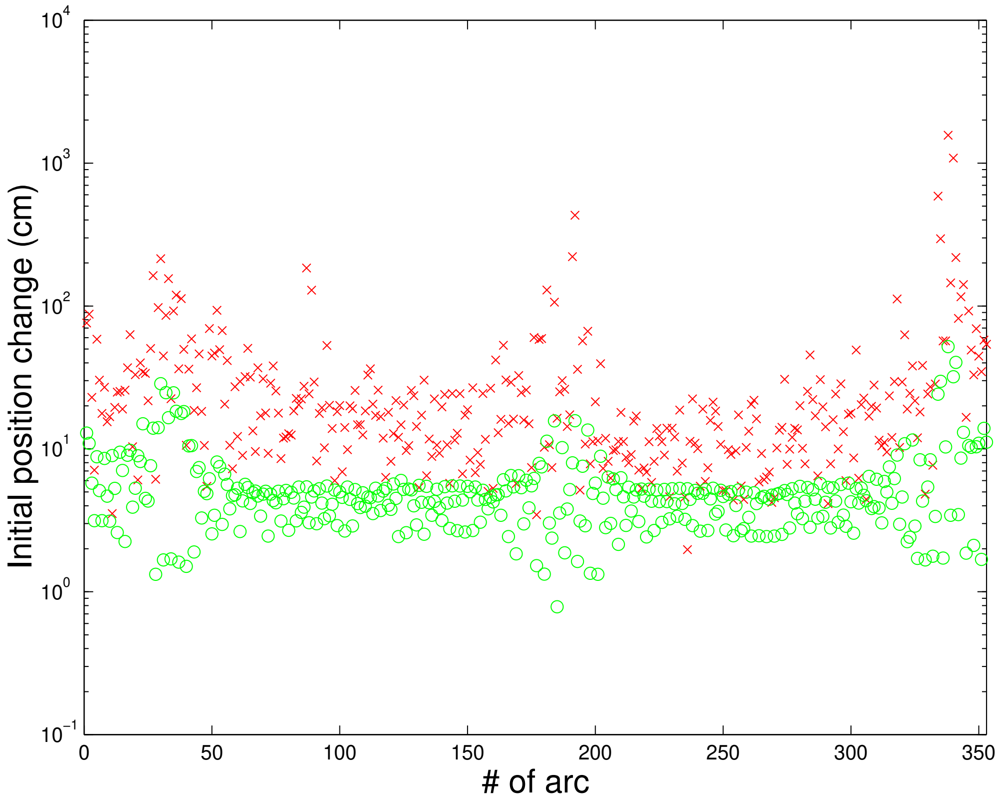

Figure 7: Formal uncertainties (circles) and actual errors (crosses) in the initial conditions determination for each arc, in the short arc case. The arcs cover one year (nominal mission duration).

In the case of the short arcs the time span is enough to allow for some angular motion of the Earth-Mercury line of sight and the rank deficiency problem is not severe; on the other hand, from Fig. 7, we note that in this case the errors lie almost all above the formal uncertainty, due to the systematic effects from non modeled nongravitational perturbations, accumulated over the time span of the short arc. In fact the RMS value of the actual errors was 123 cm for the short arcs while it was only 51 cm for the very short arcs. The loss of accuracy due to the rank deficiency is inversely proportional to the time span, while the accumulated effect of unmodeled accelerations is proportional to the square of the time span (for the along track component), thus it is clear that the ratio of the two effects can change sharply when the arc length increases. As it is apparent from Fig. 7, with the very short arcs some especially poor orbit determinations occur for a few arcs; this can be understood because the "bad" arcs are either especially short or have an especially unfavorable geometry. Some algorithm could be devised to select some arcs to be discarded, thus reducing the RMS error.

Accuracy of orbit predictions for the rotation experiment

The rotation experiment is described in Section 5; the only component of its error budget which depends upon the orbit determination process is the error in the mercurycentric position of the spacecraft. Fig. 8 shows the errors in the position of the spacecraft one day after the observations, forming one short arc, which have been used in the fit. The Figure shows only the actual errors, since the formal errors would largely underestimate the uncertainty; the RMS is 22.9 meters, for this simulation over 6 months.

However, this is an overestimate to the contribution of orbital uncertainty to the rotation experiment. We have used propagation of 24 hours for the convenience of comparing the initial conditions of each short arc with the prediction resulting from the next short arc, which is the next day. But the propagation needs to be done for no more than half that time, since it can be done both from the previous and from the following day; thus we estimate the RMS error would be less than 10 m.

4 Determination of the gravity field

The gravimetry experiment, that is the determination of the gravity field of Mercury, has been simulated by using a hypothetical gravity field obtained as follows. The mass and the degree 2 coefficients have been set to the values

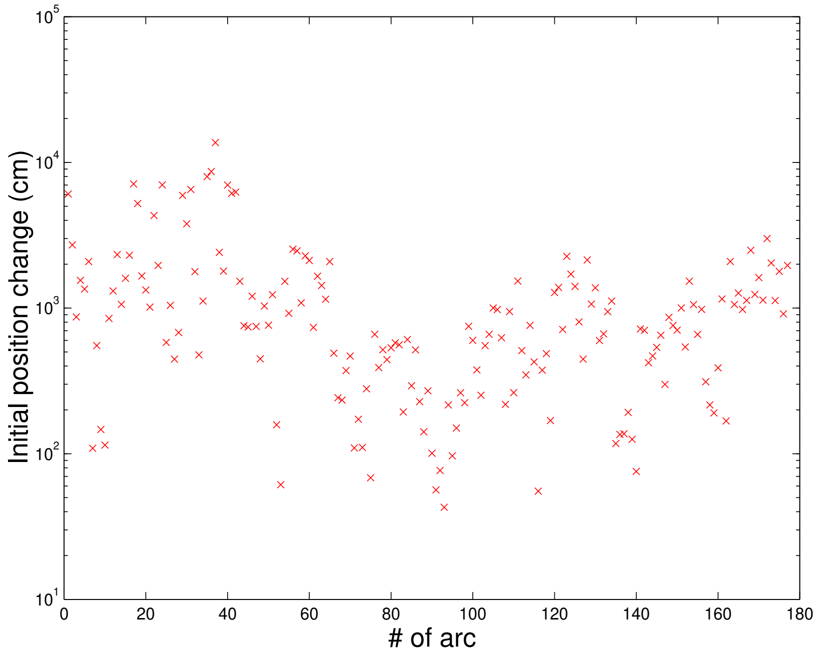

Figure 8: Uncertainty in the position knowledge of the orbiter in a mercurycentric frame (short arcs, interrupted only by the setting of Mercury below the horizon at the station). The uncertainty is computed for one day after the observations, which is more than what is required for the rotation experiment.

from Anderson *et al.* (1987). Normalized coefficients of degrees 3 to 20 have been obtained by multiplying the corresponding harmonic coefficients for the Earth by a factor 3. This simulates a gravity field following a Kaula's rule $3 \times 10^{-5}/\ell^2$ (for the RMS of the normalized coefficients of degree ℓ).

The harmonic coefficients are solved in a global least squares fit, using all the data, together with corrections to the orbit of Mercury, accelerometer calibration constants and initial conditions for each arc. The multiarc algorithm (Milani *et al.*, 1995) has the property that the correlations between the local variables (applicable only to a single arc, e.g., initial conditions) and the global variables (such as the harmonic coefficients) are taken into account, providing a consistent covariance matrix for all the variables. Nevertheless, we need to investigate the systematic errors and not only the random ones, and this has been done by comparing the values determined in the differential correction process with the "true" values used in the data simulation.

4.1 Results of the full simulation

The simulation results for the determination of the harmonic coefficients of the Mercury gravity field are summarized in Fig. 9, where the gravity signal, expressed by means of harmonic coefficients as a function of the harmonic degree ℓ, is compared with the uncertainty in the results in the formal sense (as described by the covariance matrix) and to the actual error found in the output of the simulated full cycle data processing.

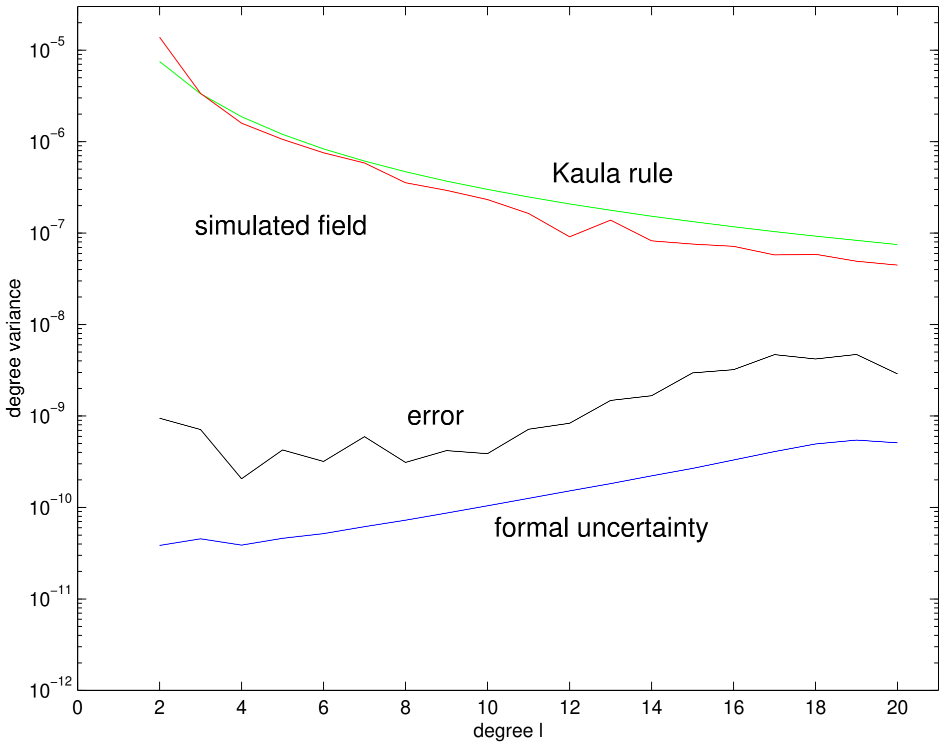

Figure 9: Results of the simulation for the determination of the coefficients of the gravity field of Mercury. As a function of the degree ℓ the four lines in the figure show, from top to bottom: the expected RMS value of the coefficients according to the well established Kaula's rule; the random values used in the simulation (degree 2 coefficients have been set to the value determined with the Mariner 10 tracking data); the actual RMS error including the systematics and the formal RMS uncertainty of the results.

As already pointed out, the assumptions used in this simulation include a full error model for both the range/range-rate observations and the accelerometer measurements, and not only white noise errors. This is why it is essential to compare the actual errors to the formal standard deviation as derived from the covariance matrix. Fig. 9 indeed shows that systematic errors are dominant; an estimate of the achievable accuracy based upon the formal covariance would be misleading by an order of magnitude, both for long and short wavelength gravity signals. The simulation has actually been performed in two ways: with *short arcs* and with *very short arcs* (see the definitions in Section 2.1). The results in Fig. 9 refer to the simulation with very short arcs; in the other case, the systematic errors were larger by a factor between 2 and 5 (depending upon ℓ), while the formal errors are essentially the same. This means that the cause of the systematic error in the results is in some incomplete modeling, not absorbed by the variables included in the solution, whose effect increases sharply with time. This is consistent with the results shown by the orbit determination in the two cases, in particular with the systematic effects apparent in Fig. 7. The most likely explanation is that this is the effect of the time dependent accelerometer calibration, while the solution contains only a calibration constant for each arc.

The results are particularly good for the medium to high resolution gravity field: the signal-to-noise ratio is still 3×10^{-3} at degree 10, and about 7 at degree 20. This means the gravity anomalies (and geoid undulations) are well determined down to a resolution (half wavelength) of 400 km, roughly equal to the minimum altitude of the spacecraft, an intuitive result indicating that the dynamical mismodeling is not degrading the results.

Fig. 10 shows, for each degree ℓ_0, the cumulative error resulting from the sum of the errors done for degrees $2 \leq \ell \leq \ell_0$. In this case they are represented as gravity anomalies on the surface of the planet; since the spherical harmonics are orthogonal, the RMS of the cumulative error in the gravity anomalies is obtained as the square root of the sum of squares. One obvious feature of Fig. 10 is that the accumulated error resulting from inaccurate determination of the coefficients up to degree 20 is much less than the signal at degree 20. This implies that the omission error resulting from truncation of the spherical harmonics expansion at degree 20 is larger than the error internal to the solution. Thus we have been too conservative in our simulation, and we should have used an expansion up to degree $\simeq 25$ to bring the omission error at the same level as the internal error. This also means that the BepiColombo data should allow to solve, with a signal-to-noise ratio larger than 1, up to degree $\simeq 25$.

The relative accuracy for the coefficients of degree 2, most important for constraining the global internal structure, is about 10^{-4}; the Love number k_2

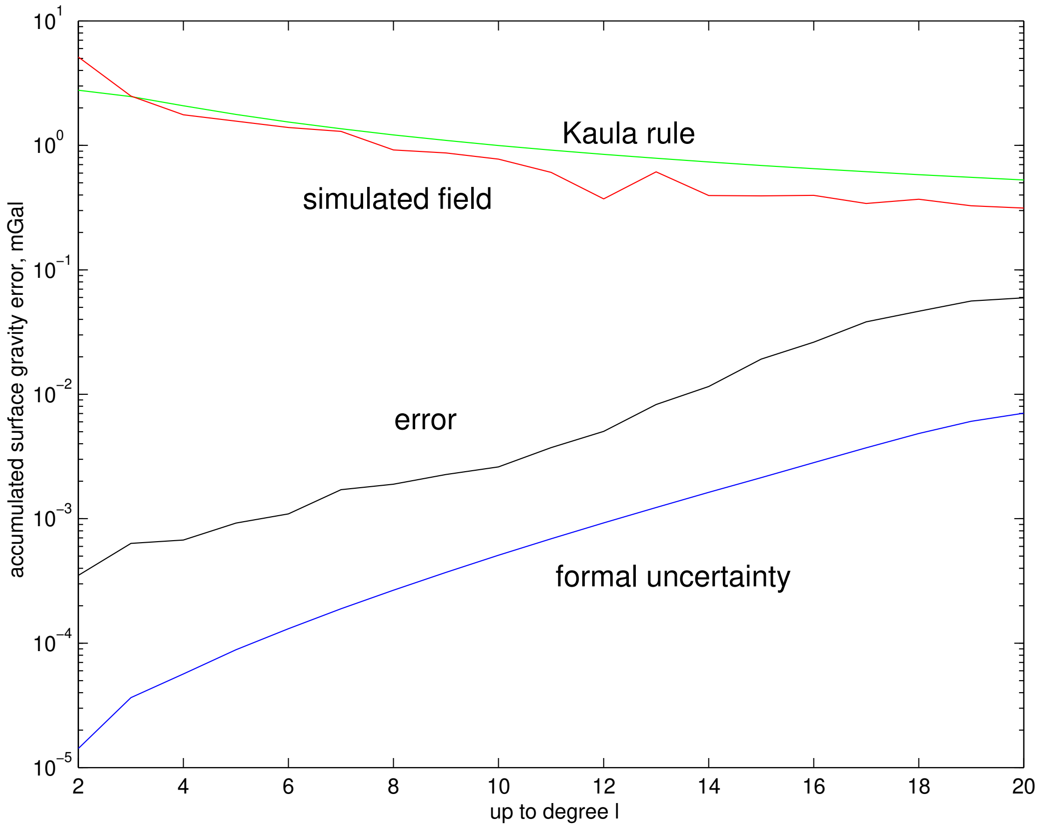

Figure 10: Results of the simulation for the gravity anomalies on the surface of Mercury. The two top lines are the signal present at each degree, the two bottom ones are the accumulated error in the gravity anomalies up to a given degree. The values are in milliGal and have to be understood as RMS over the entire surface.

is determined to a real accuracy of 6×10^{-3}. These results are satisfactory in that they are good enough to allow for very strong constraints to the models of the interior structure; only the result for the Love number is worse by a factor $\simeq 2$ than the a priori requirements of Section 1.2. The problem is, the ratio between the actual errors and the formal ones, deduced from the full covariance matrix, is very high, with a maximum at $\simeq 60$ in the case of the Love number k_2 (see Table 1). We do not fully understand the reason for such a high ratio, while this ratio is ≤ 10 for most harmonic coefficients. It appears that the cause of such large systematic errors is more in the systematic components of the accelerometer noise, rather than in the ones of the range and range-rate measurements. This is also consistent with

	Systematic error	Random error
C_{20}	-2.2×10^{-9}	1.3×10^{-10}
S_{21}	1.8×10^{-9}	4.5×10^{-11}
C_{21}	-5.1×10^{-10}	4.7×10^{-11}
S_{22}	2.3×10^{-10}	1.5×10^{-11}
C_{22}	7.5×10^{-10}	1.8×10^{-11}
k_2	-6×10^{-3}	9.7×10^{-5}

Table 1: Summary of the results for the determination of the gravity of Mercury.

the sensitivity of the systematic effects to the arc length. Obviously this is an open problem, which should be fully investigated to explore the possibility of a further improvement in the results of the gravimetry experiment.

5 The rotation experiment

The rotation of Mercury is the most peculiar among those of all the planets and satellites of our Solar System. The 2/3 resonance between the rotation period and the orbital period was discovered by direct measurement of the rotation rate with Doppler radar, and explained from the point of view of mechanical stability in a series of fundamental papers by Colombo (Colombo, 1965, 1966; Colombo and Shapiro, 1966). As proposed by Colombo, the resonant rotation of Mercury can be analyzed in terms of Cassini states, generalizing those known for the 1/1 resonance, e.g., for the Moon. In short, the rotation axis of Mercury lies in the plane defined by the vectors normal to the orbit of Mercury and normal to the mean orbital plane (which is close to the ecliptic plane), and between the two vectors which form an angle of $\approx 7^\circ$. In fact the rotation axis is much closer to the orbit normal: the obliquity η of the Mercury equator with respect to the orbital plane is estimated to be only ≈ 7 arc-minutes. The exact value of the obliquity is not known: it is a function of the concentration coefficient C/MR^2.

Because of the large eccentricity of the orbit, a forcing torque, periodic with the orbital period of Mercury, acts on the equatorial asymmetric bulge of the planet. Thus the main component of the libration induced by the nominal resonant rotation is characterized by the same period, one Mercury year, and consists of an oscillation in longitude of amplitude β. That is, the surface of Mercury is rotated with respect to an uniform rotation, with an expected displacement of amplitude $R\beta \simeq 400$ meters at the equator. The strength of the forcing torque contains the value of C_{22} and of the concentration coefficient C/MR^2; the response depends upon the value of the maximum moment of inertia C. The amplitude of the libration in longitude is small for a rigid body, and increases significantly when the surface layer (crust and mantle) is decoupled from the core; that is the moment of inertia effectively determining the amplitude of the libration is $C_m < C$, associated with the mass contained in the solid layer. Mercury, like the Earth, should have a liquid outer core, since it appears to have a dipolar magnetic field. This field is accounted for by current dynamo theories, but would be hard to explain for a completely solid planet.

The ratio of the moment of inertia of the decoupled surface layer C_m to the moment of inertia C of the entire planet (about the rotation axis) is the product of three factors:

$$\frac{C_m}{C} = \frac{C_m}{B-A}\,\frac{B-A}{MR^2}\,\frac{MR^2}{C}\,,$$

where A and B are the other principal moments of inertia. The first factor can be determined from the amplitude of the forced libration in longitude β, the second factor from the C_{22} harmonic coefficient and the third factor from the Cassini state obliquity η of the rotation axis (Peale, 1988). Each one of the three factors is by itself an important scientific objective of the mission; the expected values are $C_{22} \simeq 1.6 \times 10^{-5}$ from the Mariner 10 tracking data, $C/MR^2 = 0.34$ for the concentration coefficient (must be < 0.4) and $C_m/C = 0.5$ (both highly uncertain). The product of the three factors provides a key to understand the physical state of the interior of Mercury and the origin of its magnetic field.

The method to measure the rotation of the surface of Mercury with respect to a non-rotating frame is outlined in Fig. 11. Let G1 and G2 be the positions of the same reference point on the solid surface of Mercury at two well separated times t_1 and t_2 (for the constraints on these times, see Section 5.1). Let S1 and S2 be the positions of the spacecraft at the same times, and let O be the center of mass of Mercury. The vectors S1-O and S2-O

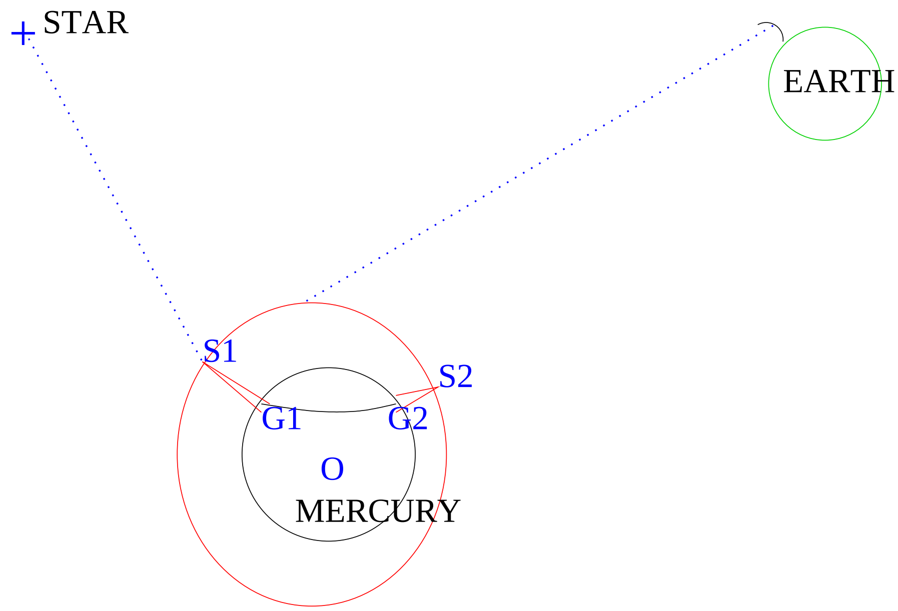

Figure 11: Geometry of the rotation experiment. The on board camera, when the spacecraft is at S1, S2, takes images of a patch on the surface of Mercury around the points G1, G2 respectively, at times selected in such a way that these two points correspond to the same place on the surface. The tracking of the spacecraft from the Earth does not need to be done simultaneously.

are measured by tracking from the Earth, in a reference frame which is by definition inertial; the vectors G1-S1 and G2-S2 are measured by the camera in a reference frame defined by the star mapper measurements. Since this second reference frame is also inertial to a very good accuracy, the absolute rotation of the reference point on the surface of the planet is obtained simply by

$$\begin{cases} G1 - O = (S1 - O) + (G1 - S1) \\ G2 - O = (S2 - O) + (G2 - S2) \ . \end{cases}$$

Of course this is a simplified account; the images do not refer to a single point on the surface, but to patches which have to be correlated, and the error in this correlation must be taken into account. The stellar reference system is realized in an imperfect way, and the camera pointing has errors. All these sources of error have to be included in the error budget discussed in Section 5.2.

5.1 Scheduling of the dedicated imaging

The measurement of the rotation of Mercury is obtained by correlating images of the same patch on the surface taken with the on-board camera at different times. We need to find at which times the imaging of the same spot will be possible, and check that these times are suitable to measure a libration with a period of one Mercury year.

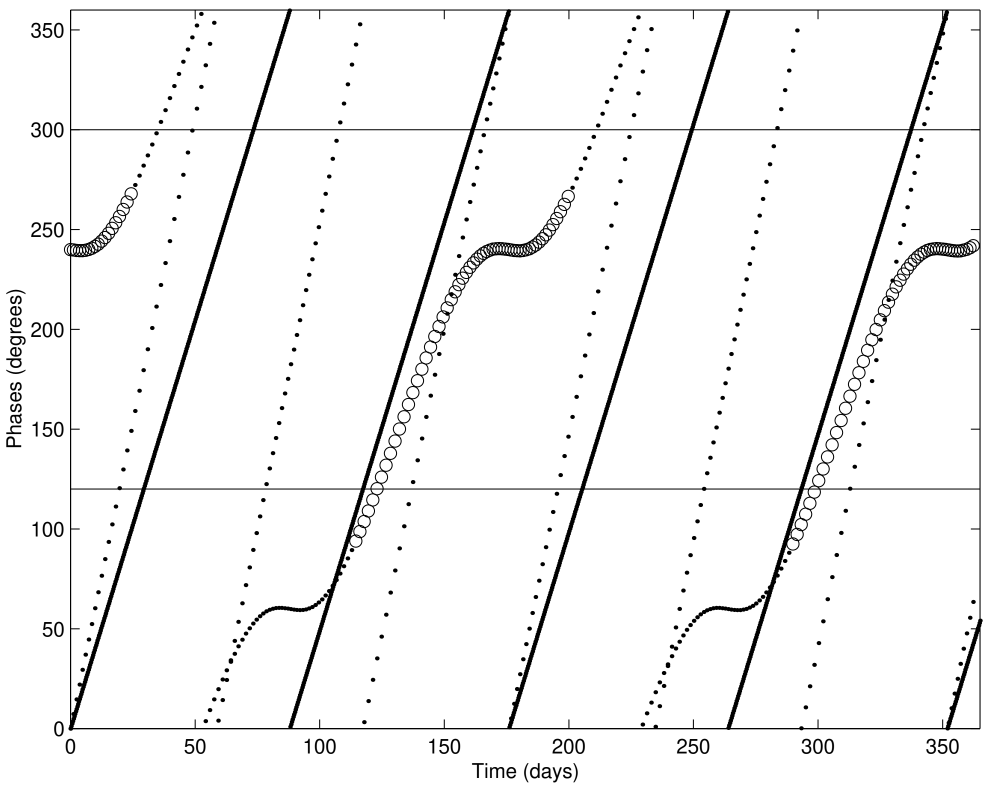

Figure 12: Visibility conditions for the rotation experiment. The slanted dotted line is the rotational phase of Mercury, the slanted solid line is the mean anomaly of Mercury. The curved line is the true anomaly of Mercury minus the rotation phase, which defines the illumination conditions: the line is drawn with small dots for illuminated conditions and with circles for non illuminated conditions (at some reference longitude). The horizontal lines indicate the location of some target longitude at the sub-satellite points in the orbital plane.

The information necessary for this task is summarized in Fig. 12. The slanted lines are the phase of the rotation of Mercury in an inertial frame (dotted) and the mean anomaly of the orbital motion of Mercury (solid). The two are in resonance, that is they are both back to the same value after exactly one *Mercury day*, corresponding to two Mercury years and three rotations of the planet. However, the illumination conditions on the surface are controlled by the true anomaly of Mercury's heliocentric orbit; because of the large eccentricity ($\simeq 0.206$) of the orbit, the mean and the true anomaly are quite different. In particular the illumination conditions are controlled by the difference between the rotation phase and the true anomaly. The curved lines in the Figure indicate the illumination phase (for a given longitude). They show the surprising property that the Sun goes back for several days in its path as seen from the surface of the planet; this occurs when the planet is near perihelion.

Taking into account that the plane of the polar orbit of BepiColombo will hardly precess, the visibility conditions from the spacecraft are represented in the Figure by two horizontal lines 180° apart; one of the two corresponds to passages closer to pericenter, the other to passages closer to apocenter, thus at a larger altitude (with imaging at a lower resolution). The opportunities to image a patch located on a given meridian are represented by the intersections of the horizontal lines with the dotted diagonal lines representing the rotation of the planet; there are 12 intersections in the nominal mission duration of one terrestrial year, corresponding to $\simeq 2$ Mercury days. However, at the times corresponding to these intersections, we need to check the illumination conditions: there will be (on average over a range of longitudes) 6 opportunities when the surface patch is illuminated.

Because of the resonance, the figure repeats exactly every Mercury day, thus for each patch on the surface there are two identical groups of (on average) 3 images. The libration in longitude has the mean anomaly as an argument, thus by correlating images taken one Mercury day apart we would obtain no information on the amplitude β of the libration. From this analysis we can draw an important conclusion: there is no way to perform the rotation experiment by correlating images with the same scale and the same illumination conditions.

The selection of the location on the surface of the patches to be repeatedly imaged for the rotation experiment cannot be entirely done a priori, but needs to take into account the local properties of the surface (Jorda and Thomas, 2001). We can assume that there would be locations distributed in longitude. As for latitude, the libration in longitude β is best measured at the equator while the obliquity η is best measured at the poles. Low latitudes would result in a too large change of scale between images taken from distances close to 400 km and close to 1500 km. At this stage of the study we can only state that some intermediate latitude should be used, but the optimal way to select the locations remains to be determined.

5.2 Error budget

The target accuracies required for a better understanding of the interior structure of Mercury, as discussed in Section 1, are

$$\begin{cases} \Delta(C/MR^2) \leq 0.003 \\ \Delta(C_m/C) \leq 0.05 \end{cases}$$

and this results in an error budget for the concentration coefficient

$$\Delta(C/MR^2) = \frac{C}{MR^2} \left[\frac{\Delta\eta}{\eta} + \Delta P\right]$$

where ΔP arises from the errors in the determination of the harmonic coefficients of degree 2; from the results of Section 4 we can conclude that this contribution is negligible. For the fraction of the moment of inertia associated with the decoupled upper layer (if any) the error budget is

$$\Delta(C_m/C) = \frac{C_m}{C} \left[\frac{\Delta\beta}{\beta} + \frac{\Delta\eta}{\eta} + \Delta P\right] .$$

From these equations we can solve for the required accuracies in β and η:

$$\begin{cases} \Delta\beta \leq 3.2 \text{ arcsec} \\ \Delta\eta \leq 3.7 \text{ arcsec} , \end{cases}$$

corresponding to displacements of the surface of 37 m at the equator for β and 43 m at the poles for η.

This error budget for $R\beta, R\eta$ must in turn be allocated to the known sources of error:

1. error in the knowledge of the position of the spacecraft in a mercurycentric non-rotating frame;

2. error in the relative position of reference points on the surface, as measured by correlating two images;

3. error in the knowledge of the pointing of the star mapper with respect to an absolute reference frame (defined by stars);

4. error in the angles defining the pointing of the camera with respect to the pointing of the star mapper.

Item 1 has been discussed in Section 3.2; the conclusion is that this error can be assumed to be < 10 meters (RMS value). Items 2, 3 and 4 have been the subject of dedicated studies.

For item 2 we rely on the conclusions of Jorda and Thomas (2001), which can be stated (in a very simplified way) as follows. The patches on the surface to be used have to be selected among those with suitable albedo and/or elevation features. The accuracy of the pattern matching, using either albedo spots or craters, can be maintained at one pixel or less, provided some conditions on the illumination angles and on their difference in the two images are satisfied. As discussed in Section 5.1, the imaging to be used for the rotation experiment cannot be performed at the pericenter, but from an altitude depending upon the selected latitude; we can assume an altitude of $\simeq 1000$ km for the one of the two images taken from higher altitude. Thus the pixel size is increased from the value at pericenter (10 m, see Balogh *et al.*, 2000, Section 3.1.2) to about 25 m.

For item 3, the accuracies of the best star mappers available now are better than 2 arcsec. From 1000 km this corresponds to 10 m on the surface.

For item 4 a dedicated study has been conducted by the prime contractor of the *System and Technology Study*, Alenia Spazio. An accommodation strategy has been found to ensure a high degree of rigidity to a common support for the narrow field camera and a star mapper. The deflection, resulting from thermo-mechanical forcing of this support, is estimated to be less than 2 arcsec, that is again 10 m on the surface.

Since these sources of error are independent, an estimate of the RMS error is obtained simply by

$$\sqrt{10^2 + 25^2 + 10^2 + 10^2} = 30.4$$

meters on the surface.

The significance of this estimate is clear: the required accuracy is achievable with a single shot measurement, that is by looking repeatedly (six times, as discussed in Section 5.1) at a single patch on the surface of Mercury.

This of course does not conclude a study of the accuracy achievable in the rotation experiment of BepiColombo, because we have yet to study how much of this error would be accidental, and therefore could be decreased simply by repeating the experiment 10, 100, maybe several hundred times (which is perfectly compatible with the data volume available). However, this is enough to show that the experiment is feasible, and that its accuracy can reach and even exceed the specifications deduced from the scientific goals stated in Section 1.2.

6 Conclusions

The results of the full cycle data simulation have confirmed that the BepiColombo Radio Science Experiments can achieve the stated science goals, and in some cases even exceed the specifications (i.e., information can be provided on the gravity anomalies down to a resolution of $\simeq 300$ km, even better than the original goal of 400 km).

This does not imply that there are no problems, and that the preparation work necessary before the mission arrives to Mercury is complete. We would like to conclude with the list of open problems which we plan to investigate.

- To find the nature of the aliasing mechanism between some systematic measurement errors (already present in our error models) and the effect of some gravity signals, especially the ones from the low order harmonics and the tidal deformations.

- In the hypothesis, which we favor, that this aliasing takes place between colored noise in the accelerometer measurement and the gravity signals, to establish whether an increase in the performance of the accelerometer would allow an overall increase in the performance of the gravimetry experiment.

- To establish whether *very short* or *short* arcs should be used in the orbit determination. For the gravimetry experiment the results of the simulation indicate that the very short arcs give better results, but for the relativity experiment the results are significantly improved by using short arcs, as discussed in Milani *et al.* (2001).

- In the context of the choice of the previous item, find the optimal way to constrain the orbit determination process, by removing the approximate degeneracies by means of information gathered over time scales longer than the arcs.
- To assess the improvement in the accuracy of the results which could be obtained by using two (or more) ground antennas, thus by processing more data, organized in much longer observed arcs.
- To study the contribution to the determination of the geophysically significant parameters which could be achieved by adding a laser altimeter to the MPO payload. The impact of this additional instrument has not been assessed yet, because it was not included in the payload used in the last spacecraft design exercice.
- To assess the problems introduced by the attitude and orbit maneuvers and determine operational control procedures which do not degrade the Radio Science Experiments and are at the same time acceptable from the point of view of mission control.
- To evaluate the improvement, with respect to the single shot accuracy, achievable in the rotation experiment by repeating the measurements on a number of different surface patches; also, to define an optimal strategy to select the location of these patches, and a corresponding schedule for the experiment, compatible with the mission constraints.

References

[1] Albertella, A. and Migliaccio F. (Eds.), 1998. SAGE, Satellite Accelerometry for Gravity field Exploration: Phase A final report, International Geoid Service, Milano, Italy.

[2] Anderson, J.D., Colombo G., Esposito P.B., Lau E.L. and Trager G.B., 1987. The mass, gravity field and ephemeris of Mercury, Icarus, 71, 337 – 349.

[3] Balogh, A. *et al.*, 2000. BepiColombo: An interdisciplinary Cornerstone Mission to the planet Mercury, ESA-SCI(2000)1.

[4] Bonanno, C. and Milani A., 2001. Symmetries and rank deficiencies in the orbit determination around another planet, in preparation.

[5] Carpino, M., Milani A. and Nobili A.M., 1987. Long-term numerical integrations and synthetic theories for the motion of the outer planets, Astron. Astrophys., 181, 182 – 194.

[6] Colombo, G., 1965. Rotational period of the planet Mercury, Nature, 208, 575.

[7] Colombo, G., 1966. Cassini's second and third laws, Astron. J., 71, 891.

[8] Colombo, G. and Shapiro I.I., 1966. The rotation of the planet Mercury, Astrophys. J., 145, 296.

[9] Iafolla, V. and Nozzoli S., 2001. Italian Spring Accelerometer (ISA): high sensitive accelerometer to be used in "BepiColombo" ESA Cornerstone, this issue.

[10] Iess, L., 2001. Ultra accurate radio tracking and the relativity experiment of BepiColombo, this issue.

[11] Jorda, L. and Thomas N., 2001. The accuracy of pattern matching techniques for the radio science experiment of ESA's Mercury Cornerstone mission, this issue.

[12] Kaula, W.M., 1966. Theory of satellite geodesy, Blaisdell, Waltham, Massachusetts.

[13] Milani, A., Carpino M., Rossi A., Catastini G. and Usai S., 1995. Local Geodesy by Satellite Laser Ranging: an European Solution, Manuscripta Geodetica, 20, 123 – 138.

[14] Milani, A., Vokrouhlický D., Rossi A., Villani D. and C. Bonanno, 2001. Test of general relativity from the BepiColombo Radio Science Experiment, in preparation.

[15] Munk, W.H. and Macdonald G.J.F., 1960. The rotation of the planet Earth, Cambridge University Press, Cambridge.

[16] Newton, I., 1687. Philosophiae naturalis principia mathematica, Ist Edition, Streater, London; for modern translation to English see Cajori F., Newton's Principia, 1934. University of California Press, Berkeley.

[17] Peale, S.J., 1976. Does Mercury have a molten core, Nature, 262, 765–766.

[18] Peale, S.J., 1988. Rotational dynamics of Mercury and the state of its core, in Mercury, Vilas F., Chapman C.R. and Matthews M.S. (Eds.), University of Arizona Press, Tucson, 461 – 493.

[19] Spohn, T., Sohl F., Wieczerkowski and Conzelmann V., 2001. The interior structure of Mercury: what we know, what we expect from BepiColombo, this issue.

[20] Vincent, M.A. and Bender P.L., 1990. Orbit determination and gravitational field accuracy for a Mercury transponder satellite, J. Geophys. Res., 95B, 21357 – 21361.

[21] Yeomans, D.K., Chodas P.W., Keesey M.S., Ostro S.J., Chandler J.F. and Shapiro I.I., 1992. Asteroid and comet orbits using radar data, Astron. J., 103, 303 – 317.